

## Absolute x-ray reflectivity study of the Au(100) surface

Doon Gibbs and B. M. Ocko

*Physics Department, Brookhaven National Laboratory, Upton, New York 11973-5000*

D. M. Zehner

*Solid State Division, Oak Ridge National Laboratory, Oak Ridge, Tennessee 37831-6024*

S. G. J. Mochrie

*AT&T Bell Laboratories, Murray Hill, New Jersey 07974-2070*

*and Center for Materials Science and Engineering, Massachusetts Institute of Technology, Cambridge, Massachusetts 02139\**

(Received 2 March 1988)

We report an x-ray scattering study of the Au(100) surface from room temperature to 1250 K. The reflected intensity, normalized on an absolute scale, has been measured along the surface-normal direction through the (002) and (022) bulk reflections. It is shown that for clean, annealed samples, (i) the Au(100) surface is atomically smooth over length scales of several thousand angstroms, (ii) the asymmetric angular dependence of the reflectivity is consistent with an expanded, possibly buckled, hexagonal overlayer, (iii) the in-plane order is not simply commensurate with the bulk, and (iv) there is a phase transition at 1170 K, which we speculate may correspond to melting of the hexagonal overlayer.

### I. INTRODUCTION

It has been known for many years that metal surfaces may reconstruct, forming a top layer of lower symmetry than the bulk. At the present time, clean surfaces which are known to reconstruct include the (100) faces of Ir, Pt, Au, Mo, and W, the (110) faces of Ir, Pt, and Au, and the (111) face of Au.<sup>1</sup> All of these have been studied by conventional surface-science techniques: low-energy electron diffraction (LEED), ion scattering, scanning tunneling microscopy (STM), and others. While significant progress has been made, many questions still remain concerning the basic structure and phase transitions exhibited by clean metal surfaces. In part, this has led to the current interest in surface studies by x-ray diffraction techniques.<sup>2-9</sup> In this paper, we present the results of an x-ray reflectivity study of the Au(100) surface between room temperature and  $T \sim 1250$  K. Our motivation in these experiments was twofold: (1) to explore the sensitivity and utility of x-ray reflectivity methods applied to a reconstructed metal surface, and (2) to investigate the importance of atomic vibrations in the scattering at elevated temperatures ( $T_m \sim 1336$  K), a regime where relatively little work has yet been done.<sup>10</sup> The choice of Au was natural in view of the possibility that the (100) surface might provide an experimental realization of the melting of an incommensurate, two-dimensional hexagonal solid upon a square substrate.<sup>11</sup> In addition, the high  $Z$  and low reactivity make gold surfaces especially attractive candidates for model x-ray diffraction studies.<sup>2</sup>

An important feature of the present work is that the data were collected on an absolute scale, normalized by

the incident x-ray intensity. Absolute reflectivity measurements impose stringent constraints on subsequent modeling. Although these techniques have found particular success in x-ray studies of liquid and liquid-crystal surfaces<sup>12-14</sup> they have not previously been applied to metal surfaces. In this paper we show that for clean annealed samples, (i) the Au(100) surface is atomically smooth over length scales of at least several thousand angstroms, (ii) the asymmetric angular dependence of the reflectivity is consistent with an expanded, possibly buckled, hexagonal top layer, (iii) the in-plane order is not simply commensurate with the bulk, and (iv) there is a phase transition at  $T = 1170 \pm 20$  K, which we speculate may correspond to hexagonal melting. Finally, because they are new, we present a careful discussion of our experimental and analytical procedures.

The surface layer of the Au(100) is believed to exhibit a buckled, slightly rotated hexagonal structure, incommensurate (in plane) with the underlying square substrate. This picture has emerged from a variety of experiments and calculations. Briefly, the diffraction pattern obtained by LEED is consistent with a large unit cell, approximately  $c(26 \times 68)$ , of hexagonal symmetry.<sup>1,15-17</sup> Unfortunately, multiple-scattering effects have made a definitive determination of the structure impossible so far. The additional  $\sim 25\%$  mass required by such a hexagonal overlayer has been detected by ion scattering.<sup>16</sup> More recently, STM and He scattering measurements have reported a large hexagonal unit cell,<sup>18</sup> and shown that it is predominantly comprised of two types of smaller, buckled domains of  $(1 \times 5)$  corrugation.<sup>18,19</sup> Relative to the bulk there is an isotropic in-plane contraction

(3.8% along the [011] and 4.4% along [01 - 1] and a 0.1° rotation of the top layer.<sup>18</sup> Subsequent molecular-dynamics calculations have further suggested the possibility of an outward expansion of the topmost two layers to accommodate the increased mass ( $\Delta d_{12} = 3.6\%$ ,  $\Delta d_{23} = 2.2\%$ ).<sup>20</sup>

## II. PROCEDURES

### A. Experimental

The present measurements were performed at Brookhaven National Laboratory (BNL) using a 12-kW rotating-anode x-ray generator with a Ge(111) monochromator set to accept Cu  $K\alpha$  radiation ( $\lambda = 1.54 \text{ \AA}$ ). The  $0.1 \times 0.5''$  diameter sample was supported within a bakeable, high-vacuum surface chamber<sup>3</sup> which itself mounts directly onto a standard 6-circle diffractometer. The base pressure of the x-ray chamber, after bakeout, was  $\sim 1 \times 10^{-9}$  torr. Sample heating was accomplished by means of a button heater (potted); the temperature was monitored both by a Chromel-Alumel thermocouple and (most reliably) by direct measurement of the lattice constant ( $\pm 10 \text{ K}$ ). After cutting and mechanical polishing, the sample mosaic at the (002) was found to be highly structured, with a width  $> 1^\circ$  full width at half maximum (FWHM). By simultaneous sputtering and annealing for three days the mosaic was observed to decrease to  $0.04^\circ$ . Clean surfaces were prepared by simultaneous  $\text{Ar}^+$ -ion bombardment (500 V and  $1 \mu\text{A}$ ) and annealing at temperatures  $\geq 500 \text{ K}$ . This procedure always yielded stable, reproducible line shapes for extended periods. Studies of the reflectivity of a deliberately contaminated surface gave qualitatively different results. LEED patterns and Auger-electron spectra were obtained on this sample in a separate vacuum chamber held at  $1 \times 10^{-10}$  torr. After cleaning, the LEED pattern obtained at room temperature reproduced published results in detail.<sup>16</sup> Further, Auger-electron spectra revealed no contamination for all the temperatures studied in this work.

### B. X-ray reflectivity

Because x rays couple weakly to condensed matter, it is straightforward to calculate the x-ray scattering cross section, and to make reliable comparison with experiment. In the Born approximation, the cross section is

$$\frac{d\sigma}{d\Omega} = r_0^2 V S(\mathbf{Q}), \quad (1)$$

where  $r_0 = e^2/mc^2$  is the Thomson radius,  $V$  is the scattering volume, and  $S(\mathbf{Q})$  is the Fourier transform of the electronic density-density correlation function. In the case of a perfectly terminated crystalline material,  $S(\mathbf{Q})$  can be expressed as either a sum over the positions of each atomic layer

$$VS(\mathbf{Q}) = \frac{4\pi^2 A}{\Gamma^2} \sum_{H,K} \delta(Q_x - \tau_x) \delta(Q_y - \tau_y) |F(\mathbf{Q})|^2 e^{-2W(\mathbf{Q})} \times \left| \sum_{n=0}^{\infty} e^{iQ_z dn} \right|^2 \quad (2)$$

or equivalently as a sum over Bragg peaks<sup>21-25</sup>

$$VS(\mathbf{Q}) = 4\pi^2 A \sum_{H,K} \delta(Q_x - \tau_x) \delta(Q_y - \tau_y) \times \left[ \frac{mF(\mathbf{Q})e^{-W(\mathbf{Q})}}{a^3} \right]^2 \times \left[ \sum_{L \text{ even}} \frac{(-1)^{L/2}}{Q_z - Lc^*} \right]^2. \quad (3)$$

In these expressions  $A$  is the illuminated area,  $\tau = (Hc^*, Kc^*, Lc^*)$ ,  $c^* = 2\pi/a$  (for a cubic lattice),  $H, K, L$  are the allowed integer indices for Bragg reflection,  $d = a/2$  is the layer spacing,  $m = 4$  is the number of gold atoms per cubic unit cell, and  $\Gamma$  is the area per atom in each plane.<sup>26</sup> The Debye-Waller factor is given by  $W(\mathbf{Q})$  and the form factor by  $F(\mathbf{Q})$ . The  $(Q_z - Lc^*)^{-2}$  tails evident in Eq. (3) are familiar in the context of Darwin theory of Bragg reflectivity. Because of the factor  $(-1)^{L/2}$ , the amplitudes of the two nearest Bragg peaks add constructively.

For interfaces which deviate from ideal termination, the reflectivity behaves differently than for a perfect lattice. In fact, the deviation can be related to the surface-density profile through simple real-space models.<sup>13,21-24</sup> We believe that changes as small as 5% in the lattice constant normal to the surface are readily observable. Robinson *et al.* have elegantly demonstrated these ideas in their studies of buried Si(111) interfaces.<sup>27</sup>

When the spectrometer is set to accept a given  $H$  and  $K$ , the measured reflectivity  $R$  is given by the differential cross section integrated over the range of angles accepted by the detector. It is also necessary to normalize to the incident beam area and take into account the x-ray polarization. The total number of counts within the resolution volume must be given by the number of incident x-rays. The latter determines the weighting of the resolution function to be  $(\Delta\theta_1)^{-1}$ , so that

$$RA_0 = \frac{P}{\Delta\theta_1} \int (d\sigma/d\Omega) d\Omega, \quad (4)$$

where  $P$  is the polarization factor<sup>28</sup> and  $\Delta\theta_1$  is the spread of the incoming beam. Equation (4) is strictly correct if the incident x-rays are uniformly distributed over  $\Delta\theta_1$ . The extension to the more general case, however, is straightforward.<sup>14</sup> Using Eqs. (2) and (4), we find

$$RA_0 = \frac{4\pi^2 r_0^2 A L_0 P}{\Gamma^2 \Delta\theta_1} |F(\mathbf{Q})|^2 e^{-2W(\mathbf{Q})} \left| \sum_{n=0}^{\infty} e^{iQ_z dn} \right|^2 \Delta Q_z. \quad (5)$$

$\Delta Q_z$  is the extent of the reflectivity that falls within the resolution volume.  $L_0 = [k^3 \sin^2(2\theta)]^{-1}$  is the usual Lorentz factor relating a volume in reciprocal space to one in real space. In the case of specular reflectivity  $A = A_0/\sin\theta$ , and it is straightforward to see from Fig. 1 that  $\Delta Q_z = 2k \cos\theta \Delta\theta_1$ . The nonspecular case is slightly more complicated: when the surface normal ( $\hat{n}$ ) lies in the plane of the scattering vector and of the  $\theta$ - $2\theta$ -diffractometer axis, the incident and exit angles ( $\alpha$ ) from

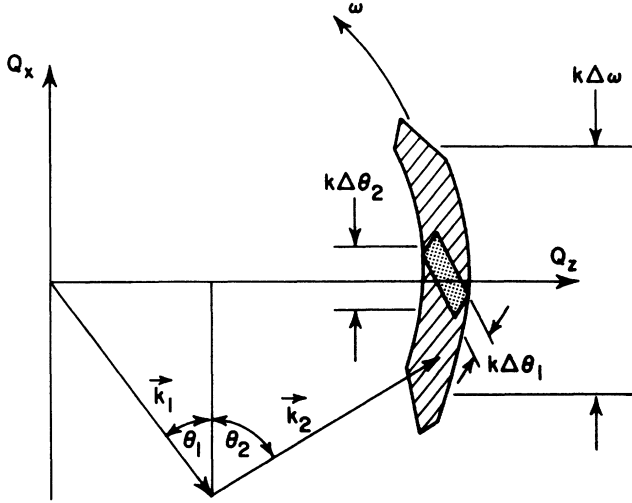


FIG. 1. X-ray resolution volume projected onto the scattering plane. The shaded area is the resolution trapezoid defined by the spread of the incoming beam ( $\Delta\theta_1$ ) and the acceptance of the detector slit ( $\Delta\theta_2$ ). The resolution area swept out by scanning  $\omega$  over a range  $\Delta\omega$  is given by the hatched arc.

the sample surface are equal. For convenience we chose to impose this constraint upon the diffractometer settings during the experiment. In this case, the reflectivity is tilted at an angle  $\arccos(\hat{\mathbf{n}} \cdot \hat{\mathbf{Q}})$  with respect to the scattering plane. ( $\hat{\mathbf{Q}}$  is the unit vector parallel to the scattering vector.) Therefore,  $\Delta Q_z = 2k \cos\theta \Delta\theta_1 / \hat{\mathbf{n}} \cdot \hat{\mathbf{Q}}$ . Using  $A = A_0 / \sin\alpha$  we obtain from Eq. (5),

$$R = \frac{4\pi^2 r_0^2 |F(\mathbf{Q})|^2 e^{-2W(\mathbf{Q})}}{\Gamma^2 k^2 \sin\alpha (\hat{\mathbf{n}} \cdot \hat{\mathbf{Q}} \sin\theta)} \left| \sum_{n=0}^{\infty} e^{iQ_z dn} \right|^2. \quad (6)$$

For equal incident and exit angles  $\hat{\mathbf{n}} \cdot \hat{\mathbf{Q}} \sin\theta = \sin\alpha$ ,<sup>29</sup> and the final expression for the off-axis reflectivity becomes

$$R = \frac{4\pi^2 r_0^2 |F(\mathbf{Q})|^2 e^{-2W(\mathbf{Q})}}{\Gamma^2 k^2 \sin^2\alpha} \left| \sum_{n=0}^{\infty} e^{iQ_z dn} \right|^2. \quad (7)$$

The equivalent form, corresponding to Eq. (3), follows immediately as

$$R = \frac{4\pi^2 r_0^2 |F(\mathbf{Q})|^2 e^{-2W(\mathbf{Q})}}{\alpha^4 k^2 \sin^2\alpha} (m/a)^2 \left| \sum_{L \text{ even}} \frac{(-1)^{L/2}}{Q_z - Lc^*} \right|^2. \quad (8)$$

Since for specular reflection  $\alpha = \theta$ , Eqs. (7) and (8) can also be used for specular reflectivity. Equations (7) and (8) are valid provided that (i) the detector slits are sufficiently open that the longitudinal resolution is defined only by the incoming angular divergence, (ii) the input slits define the illuminated sample area, (iii)  $\alpha$  is large enough that refraction effects may be safely ignored, (iv) the sample is sufficiently flat, and (v) the incident and exit angles are equal.

### C. Nonideal samples

The x-ray beam size was controlled by a defining slit located close to the sample. The finite x-ray source size on the anode collimated the incoming beam in the scattering plane to  $\Delta\theta_1 = 0.001^\circ$  FWHM for the narrowest slits. This in turn produced a minimum beam width at the sample position of 0.1 mm. The spectrometer resolution (see trapezoid in Fig. 1) was determined by the divergence of the incoming x-ray beam and the acceptance of the scattered x rays by the detector slit. In the scattering plane, the outgoing divergence ( $\Delta\theta_2 = 0.05^\circ$  FWHM) was fixed by the detector slit width. Out of the scattering plane, the resolution was  $\Delta\chi_2 = 1.0^\circ$  FWHM.

For perfectly flat and crystallographically aligned samples, the acceptance angle of the detector need only be as large as  $\Delta\theta_1$  to collect all of the reflected intensity. However, for nonideal samples the scattering is distributed over a range of exit angles determined by the sample mosaic. In order to properly integrate over this mosaic the transverse resolution must be broader than the features of the mosaic. The in-plane resolution can be coarsened by increasing the detector width ( $\Delta\theta_2$ ), although there is a simultaneous decrease in the longitudinal resolution. In order to maintain good longitudinal resolution we have chosen to integrate over a range of  $\omega = \theta - (2\theta)/2$  at constant  $2\theta$ , by rocking the sample as shown by the arc in Fig. 1. Under these conditions, the reflectivity is given by

$$R = \frac{\int d\theta I_s(\theta)}{\frac{1}{2} \int d(2\theta) I_0(2\theta)}, \quad (9)$$

where  $I_s(\theta)$  is the scattered intensity after background subtraction and  $I_0(2\theta)$  is the direct-beam intensity. The improved longitudinal resolution is crucial for the accurate measurements of the lattice constant which were used to measure the sample temperature.

### III. RESULTS AND ANALYSIS

Figure 2(a) displays the specular reflectivity of Au(100) from  $Q_z/c^* = 0.15$  to  $Q_z/c^* = 3.5$  at  $T = 310$  K. The inset shows a typical rocking curve obtained at the anti-Bragg position ( $Q_z/c^* = 1.0$ ) at this temperature. Before turning to a more detailed analysis, it is worth noting that the measured reflectivity in Fig. 2 extends over a range of nearly seven decades and over scattering angles from  $2\theta = 1^\circ$  to  $75^\circ$ , smoothly joining the (002) reflection to the origin. This is all the more impressive in view of the finite reflectivity obtained at the "forbidden" (001) reflection, where successive planes scatter exactly out of phase. Together with the absence of any measurable diffuse scattering in the transverse direction this suggests that on the length scales sampled by the resolution volume, the surface may be both atomically flat and perfectly aligned with the crystallographic planes. To estimate the in-plane coherence area we note that the width of the  $\theta$  scan [inset to Fig. 2(a)] is only  $0.07^\circ$  FWHM. This corresponds to the  $2\theta$  resolution and gives a width in reciprocal space of  $\Delta Q_x = Q_z \Delta\omega = 0.001 \text{ \AA}^{-1}$ . The center of the rocking curve remains aligned with the (002)

direction to within  $0.01^\circ$  from  $Q_z/c^* = 0.1$  to 3.5. This is comparable to the uncertainties of the Huber 5020 goniometer.<sup>30</sup> Because it is very unlikely that a Au surface can be cut to these specifications, we conclude that (upon annealing) it must rearrange itself to expose smooth (100) facets several thousand angstroms across. This observation is in agreement with the remark of Rottman and Wortis<sup>31</sup> that the rounded regions of the gold equilibrium crystal shape at  $T_m$  meet the (100) facets at a finite angle, implying that there is a range of disallowed orientations near the [100] direction. It seems certain that the several thousand angstroms correlation length is a lower limit because of the contributions to  $\Delta\omega$  of “extrinsic” factors, such as the macroscopic sample mosaic ( $0.02^\circ$ ) and the finite  $2\theta$  resolution. Finally, we remark that as excellent as it is, the sample exhibits a slight

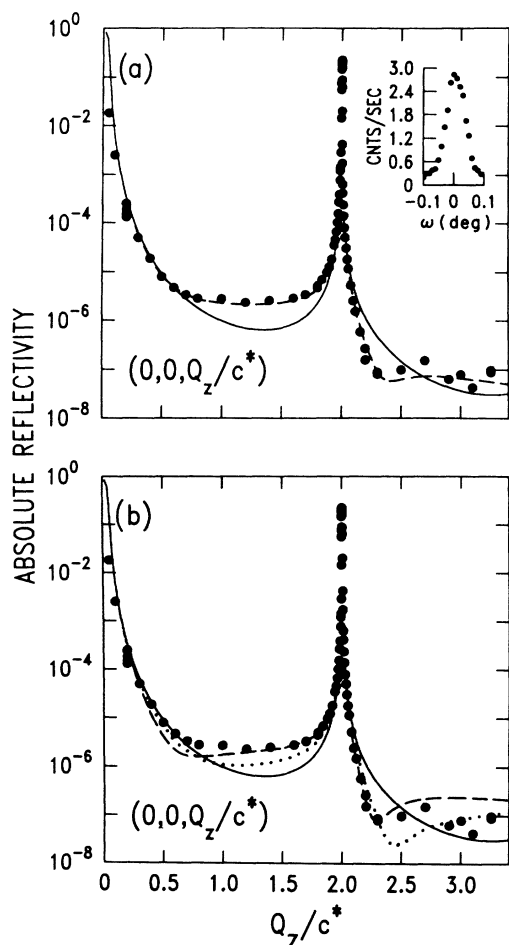


FIG. 2. (a) Specular reflectivity of the clean Au(100) surface normalized to the incident flux. The solid circles are at  $T = 310$  K. The solid line corresponds to a real-space model with an ideally terminated bulk as given by Eq. (6). The dashed lines correspond to  $\epsilon_0 = 19\%$ , an increased mass of  $\Delta\rho_0 = 25\%$ , and a buckling amplitude of  $\xi_0 = 20\%$  as described by Eq. (10). The inset corresponds to the rocking curve at  $Q_z/c^* = 1.0$ . (b) The measured reflectivity at  $T = 310$  K (solid circles) is compared to the ideally terminated bulk reflectivity (solid line). The dotted and dashed lines show, respectively, the reflectivity with  $\epsilon_0 = 9\%$  and  $21\%$ .

macroscopic curvature (figure error), which complicates absolute measurements at angles below the critical angle ( $\alpha_c = 0.57^\circ$ ).

The most striking feature of the data in Fig. 2(a) is the pronounced asymmetry evident in the reflectivity about the (002) reflection. Some of this arises from the Lorentz and form factors, and some from the variation of the illuminated area with angle. Taking these into account, however, the measured profile still cannot be described as resulting from an ideally terminated gold crystal. The solid line in Fig. 2(a) was obtained from Eq. (7) using the known atomic and crystal structure of bulk Au. It is clear that the model's prediction is substantially too low for  $Q_z/c^* < 2$  and too high for  $Q_z/c^* > 2$ . Nor can the asymmetry be qualitatively understood as resulting from surface damage or contamination. In the first place the reflectivity at the anti-Bragg position from a rough surface is generally reduced from that of a smooth surface,<sup>21,23,24</sup> which is clearly not supported by the data. More directly, Fig. 3 displays the reflectivity profiles obtained from a clean surface at room temperature (solid circles), a clean surface which has been exposed to atmosphere for  $> 24$  h and then heated in vacuum to 690 K (open squares), and a freshly sputtered (50 min) clean surface (solid triangles). In both latter cases the intensity at the anti-Bragg position falls by about 1 order of magnitude, dramatically altering the original asymmetry. These two line shapes have, in fact, intriguingly similar

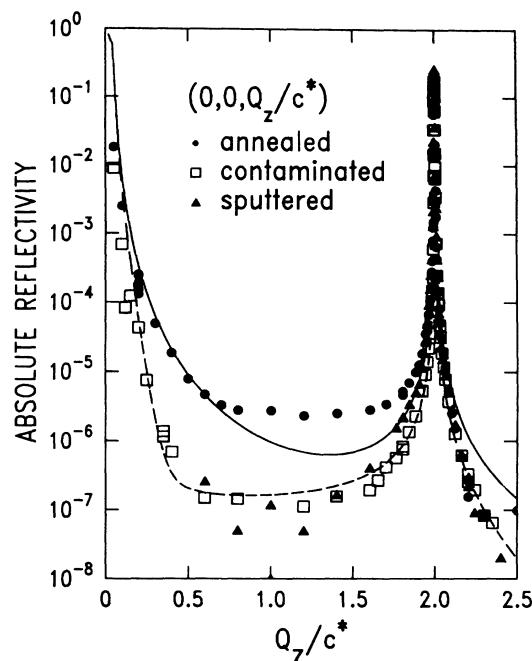


FIG. 3. Specular reflectivity of the clean Au(100) surface at room temperature (solid circles), of a surface exposed to atmosphere for  $> 24$  h and then heated to 690 K (open squares), and of a clean surface sputtered for 50 min at  $T = 300$  K (solid triangles). The solid line corresponds to the ideally terminated bulk. The dashed line is the result of a fit to Eq. (12) as described in the text.

characteristics, suggesting the possibility that the contaminated surface is also disordered. The profile of the clean surface is quickly recovered on an absolute scale for both the sputtered and contaminated surfaces by sputtering and annealing to  $T > 500$  K.

A detailed x-ray solution of the Au(100) surface structure will require synchrotron-based in-plane studies. It is nevertheless worth asking whether the observed asymmetry can be described within the simple models of the surface reconstruction. In the following we consider three different possibilities: (1) a variable spacing between the top and second layers, (2) a variable top-layer mass density, and (3) a layer-dependent out-of-plane buckling. We modify Eq. (7) by rewriting the sum as

$$R = \frac{4\pi^2 r_0^2 |F(\mathbf{Q})|^2 e^{-2W(\mathbf{Q})}}{\Gamma^2 k^2 \sin^2 \alpha} \times \left| \sum_{n=0}^N f_n(Q_z) (1 + \Delta\rho_n) e^{iQ_z d(n + \epsilon_n)} + \sum_{n=N+1}^{\infty} e^{iQ_z dn} \right|^2. \quad (10)$$

$\Delta\rho_n$  is the fractional excess mass density of the  $n$ th layer,  $\epsilon_n$  is the fractional change in the  $n$ th layer position, and  $N$  is the number of reconstructed layers. In most of our fits, we have allowed only the top layer to participate in the reconstruction ( $N=1$ ). Here  $f_n(Q_z)$  represent the Fourier transform of the charge distribution for the  $n$ th layer. For a single buckled layer in the specular geometry

$$f_n(Q_z) = J_0(Q_z \zeta_n), \quad (11)$$

where  $J_0$  is the zeroth-order Bessel function and  $\zeta_n$  is the buckling amplitude.<sup>32,33</sup> This form distributes the charge along the surface-normal direction by introducing a sinusoidal mass distribution in  $z$  into the  $n$ th layer, while preserving the center of mass of the layer. For small  $\zeta_n$ , i.e.,  $Q_z \ll \zeta_n^{-1}$ , the Bessel function and a Gaussian [ $f_n(Q_z) = e^{-Q_z^2 \zeta_n^2 / 2}$ ] are both quadratic and differ only by a scale factor. Best fits to both forms are indistinguishable over the  $Q_z$  range of the existing data. Since the Bessel-function form is motivated by a simple real-space model, we have chosen to use this form in the analysis. From the present data it is not possible to determine the sine wave period. We have also included a bulk Debye-Waller factor  $W(\mathbf{Q}) = -Q^2 \langle u^2 \rangle / 2$  with  $\langle u^2 \rangle^{1/2}$  varying between 0.1 and 0.2 Å. Such values are appropriate for bulk Au in the temperature range studied.

Because of the large range of the reflectivity and the systematic errors occurring near the Bragg peaks, the weights were determined from the inverse of the total number of counts at each point. Points within  $0.02 Q_z / c^*$  of the Bragg peak were omitted from the analysis since the weak-scattering limit implicit in Eq. (1) no longer applies in this region. Two fitting schemes were applied, both including and excluding the data above  $Q_z / c^* = 2.4$ , in order to isolate possible artifacts deriving from the relative weakness of the intensities observed in that region.

The most important result from the least-squares fitting is that of the three parameters, top- and second-

layer separation, top-layer density, and top-layer buckling amplitude, only variation of the top- and second-layer separation can produce the observed asymmetry. The effect on the reflectivity of an outwardly expanded top layer is illustrated in Fig. 2(b). No excess density nor buckling of the top layer is allowed. The line shape for the 9% expansion (dotted line) is the best fit obtained from all of the data through  $Q_z / c^* = 3.5$ , while the line shape for the 21% expansion (dashed line) is the best fit obtained excluding the data above  $Q_z / c^* = 2.4$ , where the measured intensity is weak. It is clear that while each of these introduces the required asymmetry relative to the ideally terminated bulk (solid line), neither alone provides an adequate description of the data. The dashed line in Fig. 2(a) shows the best fit obtained by varying  $\Delta\rho_0$ ,  $\epsilon_0$ , and  $\zeta_0$  (and including the data above  $Q_z / c^* = 2.4$ ). This model, which gives an excellent fit, has an expansion of  $\epsilon_0 = 19\%$ , an increased mass of  $\Delta\rho_0 = 25\%$ , and a buckling amplitude of  $\zeta_0 = 20\%$ . It is noteworthy that the deduced buckling and increased mass density are consistent with the results of earlier STM,<sup>18</sup> ion scattering,<sup>16</sup> and He scattering measurements<sup>19</sup> and with the proposed model of a buckled, hexagonal overlayer. We emphasize, however, that in view of the sensitivity of the fits to the chosen weighting scheme, these values are to be regarded as qualitative. It nevertheless seems inescapable that within the set of parameters considered here the top-layer distance is increased by an amount of the order of 20%. Considering the 25% increase in mass density of the top layer, even a 20% expansion results in a small, net increase of the volume density within the reconstructed surface region. This is consistent in magnitude and direction with the change in volume density observed in most LEED and ion scattering investigations of clean metal surfaces which exhibit multilayer relaxation.<sup>34</sup> Extending the depth of reconstruction may provide a profitable direction for future analysis, particularly involving in-plane studies.

One conclusion from the STM study of the Au(100) surface<sup>18</sup> was that the hexagonal overlayer was incommensurate with the underlying square substrate, and "floating" in the sense that a sharp domain wall description was not appropriate. Even without performing in-plane diffraction measurements it is still possible to determine whether or not the overlayer is simply commensurate by examining the asymmetry of the nonspecular reflectivity in the neighborhood of, for example, the (022) Bragg peak. This is because even if the topmost layer has an arbitrary structure, it must contribute to the specular reflectivity (for which  $Q_x = Q_y = 0$ ) since all structures have a  $Q_x = Q_y = 0$  component of their density. However, only commensurate structures with density modulations at  $Q_x = 0$  and  $Q_y = 2c^*$  can contribute to the  $(0, 2, Q_z / c^*)$  profile. Figure 4 shows a comparison between the specular and nonspecular reflectivities at  $T = 310$  K plotted on the same scale. It is unambiguous that the wings of the scattering about the (022) reflection are symmetric, while the wings about the (002) are not. This suggests that the reconstructed overlayer cannot be simply commensurate with the bulk. The solid line through the wings of the (002) reflection in Fig. 4(a) was calculated using the pa-

rameters obtained above. The best fit for the off-axis reflectivity was obtained by allowing the second- to third-layer separation  $\epsilon_1$  and the second-layer buckling  $\zeta_1$  to vary (assuming no contribution from the top layer). The results are shown by the solid line in Fig. 4(b) with  $\epsilon_1 = -3.5 \pm 2\%$  and  $\zeta_1 = 18 \pm 3\%$ . This analysis *assumes* that only the topmost layer participates in the hexagonal reconstruction.<sup>35</sup>

It is interesting that no surface roughness has been required to fit the data, supporting the suggestion that the clean, annealed surface is atomically smooth over regions of at least several thousands of angstroms in extent. In contrast, one would expect roughness to be important in a description of damaged or contaminated surfaces. Examples of these are shown in Fig. 3. The reflectivity is very much lower near the antiphase position than for the clean room-temperature data. Near the Bragg peak the two data sets agree more closely, although not perfectly. Initial attempts to analyze this data allowed for a variable

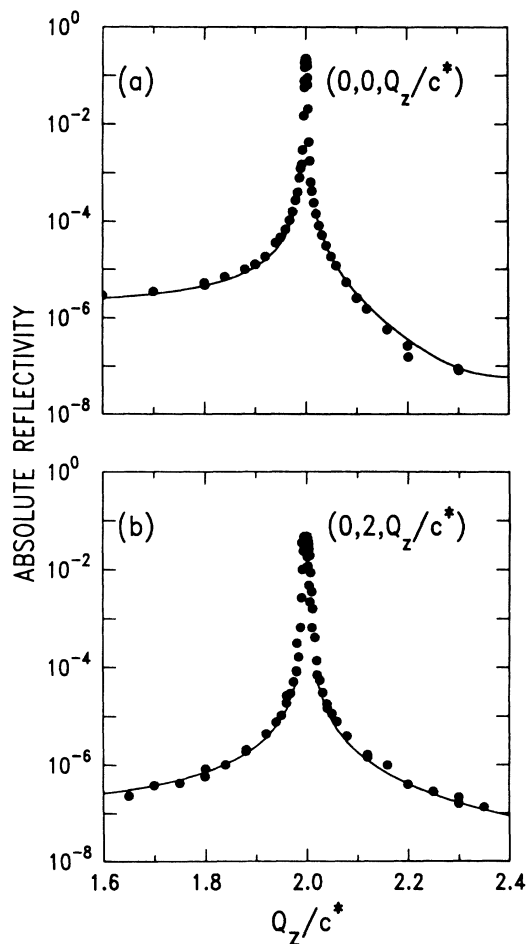


FIG. 4. Comparison between (a) specular  $(0,0,Q_z/c^*)$  and (b) nonspecular  $(0,2,Q_z/c^*)$  reflectivities vs  $Q_z/c^*$  at  $T=310$  K. The solid line in (a) is the calculated specular reflectivity of the reconstructed hexagonal overlayer with  $\epsilon_0=19\%$ , an increased mass of  $\Delta\rho_0=25\%$ , and a buckling amplitude of  $\zeta_0=20\%$  as described by Eq. (10). The solid line in (b) is the calculated nonspecular reflectivity for  $\epsilon_1 = -3.5\%$  and  $\zeta_1 = 18\%$ .

occupation in the density of successive layers, for example, according to an error-function distribution. For this model, no choice of parameters could explain the data adequately in the region between the origin and the first Bragg peak. Such a model does not fully incorporate the notion of a *damaged* surface layer. Rather than construct an elaborate real-space model, we have chosen to use a modified form of Eq. (8):

$$R = \frac{4\pi^2 r_0^2 |F(\mathbf{Q})|^2 e^{-2W(\mathbf{Q})}}{a^4 k^2 \sin^2 \alpha} \times \left| \frac{e^{-\sigma_0^2 Q_z^2/2}}{Q_z} - \frac{e^{2\pi i \phi} e^{-\sigma_2^2 (Q_z - 2c^*)^2/2}}{Q_z - 2c^*} \right|^2 (m/a)^2. \quad (12)$$

The sum is restricted to include just two charge-density waves, one corresponding to  $Q_z=0$  and the other corresponding to  $Q_z=2c^*$ , which should be sufficient in the region relevant to our experiments. Each, however, is modified by its own Gaussian of widths,  $\sigma_0$  and  $\sigma_2$ , respectively. In simple models,<sup>14</sup>  $\sigma_0$  can be identified with the root-mean-square (rms) roughness of the interface between the metal and the vacuum, while  $\sigma_2$  is the rms roughness of the interface between the ideally terminated crystal and the overlayer above it. We allow for a variable phase  $\phi$  which for perfect termination is zero [Eq. (8)]. The fit of the reflectivity data from a surface ex-

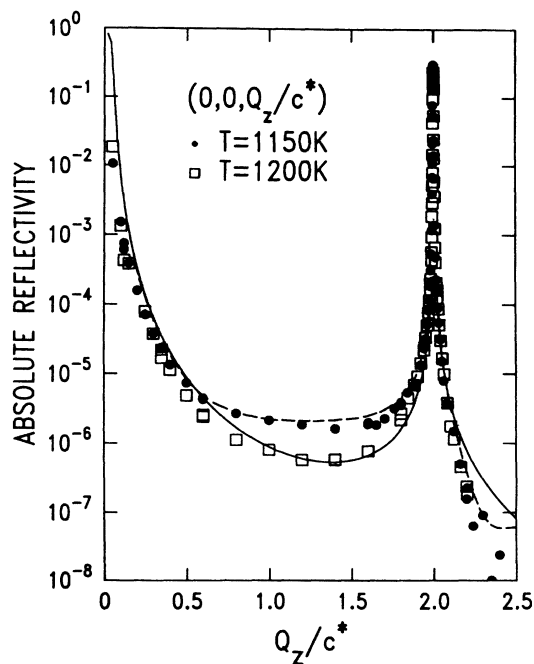


FIG. 5. Specular reflectivity of the Au(100) surface at  $T=1150$  K (solid circles) and  $T=1200$  K (open squares). The dashed line corresponds to the calculated reflectivity for the hexagonal overlayer with  $\epsilon_0=0.19$ , an increased mass of  $\Delta\rho_0=25\%$ , and a buckling amplitude of  $\zeta_0=20\%$  as described by Eq. (10). The solid line corresponds to the ideally terminated bulk with a Debye-Waller factor with  $\langle u^2 \rangle^{1/2} \sim 0.22$  Å.

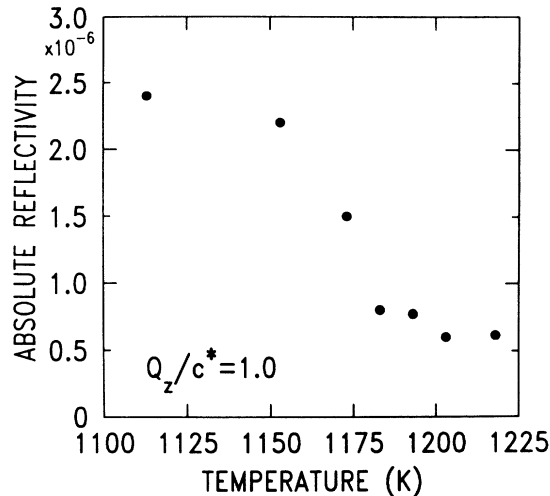


FIG. 6. Reflectivity at the anti-Bragg position ( $Q_z/c^* = 1.0$ ) vs temperature.

posed to air for >24 h (open squares) to this form (dashed line) is shown in Fig. 3. The best-fit parameters are  $\phi=0$ ,  $\sigma_0=4.5$  Å,  $\sigma_2=0.5$  Å, and  $\langle u^2 \rangle^{1/2}=0.25$  Å. Thus we arrive at the physically appealing picture of a damaged, rough surface layer (4.5 Å rms roughness), in which Au atoms are not positioned in lattice planes and are separated from the undamaged bulk by a relatively smooth interface (0.5 Å rms roughness).

The discussion to this point has focused on the room-temperature data. In fact, between room temperature and  $T=1150$  K the measured reflectivity changes very little, with the evolution of the line shape reasonably accounted for by the continuous variation of the Debye-Waller factor from about 0.1 to 0.2 Å. At  $T=1170$  K, however, the (100) surface undergoes a structural phase transition, characterized by a dramatic decrease ( $\times 5$ ) in the absolute reflectivity near the anti-Bragg position. Representative line shapes at 1150 and 1200 K are shown in Fig. 5 and the detailed temperature dependence at the anti-Bragg position is shown in Fig. 6. It is important to note that the observed change is reversible and independent of the sample's immediate history. There is no discernible change in the transverse line shape (see Fig. 7) and the reflectivity remains aligned to the surface normal (002). Most importantly, the measured reflectivity does not fall to zero at any temperature. Indeed, simple modeling reveals that for  $Q_z/c^* < 2$  the line shape is remarkably similar to the symmetric profile of the ideally terminated bulk with a Debye-Waller factor of  $\sim 0.25$  Å (see solid line, Fig. 5). The fit can be improved by introducing a small expansion. It seems unlikely that the transition is associated with surface roughening or contamination. Auger-electron spectra obtained in a UHV system on this sample at 1200 K has explicitly removed the possibility that the transition is related to surface contamination from bulk impurities. Instead, we suggest that it may correspond to melting of the hexagonal overlayer to a structure with  $(1 \times 1)$  symmetry. In this scenario the structure of the Au(100) surface is hexagonal

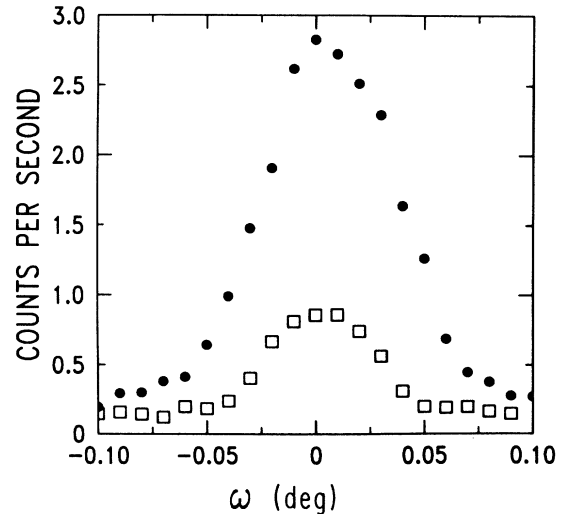


FIG. 7. Typical rocking curves at  $Q_z/c^* = 1$  taken at  $T=310$  K (solid circles) and 1200 K (open circles). The FWHM of  $0.07^\circ$  and the surface orientation are unchanged between  $T=310$  and 1220 K.

at temperatures below  $\sim 1170$  K, but transforms to a  $(1 \times 1)$  structure near the bulk melting temperature, nevertheless remaining a smooth facet. This possibility is consistent with the observation by scanning electron microscopy<sup>10</sup> that only (100) and (111) facets exist on the equilibrium crystal shape of Au near  $T_m$ . This observation is also consistent with the disappearance of extra reflections in previous LEED studies.<sup>17</sup> Clean  $(1 \times 1)$  structures have also been formed on Au(100) surfaces at room temperature by sputtering in  $O_2$ .<sup>36</sup> These, however, are metastable and irreversibly transform to the usual hexagonal structure upon heating to 400 K.

#### IV. CONCLUSIONS

In summary, by the use of the absolute-reflectivity techniques we have shown that atomically smooth Au(100) facets may be prepared over length scales of several thousand angstroms. The asymmetric angular dependence of the specular reflectivity below 1170 K is consistent with an expanded, possibly buckled, hexagonal surface structure. A more sophisticated analysis of the out-of-plane structure will accompany future in-plane studies. The lack of pronounced asymmetry in the non-specular reflectivity confirms that the overlayer is not simply commensurate with the bulk. At 1170 K the surface undergoes a structural phase transition marked by a reduced asymmetry in the specular reflectivity, as would be expected for a  $(1 \times 1)$  structure. We speculate that the transition may correspond to melting of the hexagonal overlayer upon the underlying square substrate.

#### ACKNOWLEDGMENTS

We have benefited from helpful conversations with John Axe, Denis McWhan, Ian Robinson, and Hoydoo

You. We thank G. W. Ownby for assistance in preparing the sample and Al Roberts in the design of the sample holder. One of us (S.G.J.M.) acknowledges the hospitality of Brookhaven National Laboratory during these experiments. The work performed at Brookhaven is supported by the Division of Materials Research, Office of Basic Energy Sciences, U.S. Department of Energy, under Contract No. DE-AC02-76CH00016. The work per-

formed at Oak Ridge National Laboratory is supported by the Division of Materials Research, Office of Basic Energy Science, U.S. Department of Energy, under Contract No. DE-AC02-84OR21400. Work performed at MIT is supported by the National Science Foundation (Materials Research Laboratory Program) under Grant No. DMR-84-18718.

\*Present address.

<sup>1</sup>M. A. Van Hove, R. J. Koestner, P. C. Stair, J. B. Biberian, L. L. Kesmodel, I. Bartos, and G. A. Somorjai, *Surf. Sci.* **103**, 189 (1981).

<sup>2</sup>I. K. Robinson, *Phys. Rev. Lett.* **50**, 1145 (1983).

<sup>3</sup>S. G. J. Mochrie, *Phys. Rev. Lett.* **59**, 304 (1987).

<sup>4</sup>P. S. Pershan and J. Als-Nielsen, *Phys. Rev. Lett.* **52**, 759 (1984).

<sup>5</sup>J. Bohr, R. Feidenhansl, M. Nielsen, M. Toney, R. L. Johnson, and I. K. Robinson, *Phys. Rev. Lett.* **54**, 1275 (1985).

<sup>6</sup>J. W. Chung, K. E. Lutterodt, E. D. Specht, R. J. Birgeneau, T. J. Estrup, and A. R. Kortan, *Phys. Rev. Lett.* **59**, 2192 (1987).

<sup>7</sup>G. A. Held, J. L. Jordan-Sweet, P. M. Horn, A. Mak, and R. J. Birgeneau, *Phys. Rev. Lett.* **59**, 2075 (1987).

<sup>8</sup>K. S. Liang, E. B. Sirota, K. L. D'Amico, G. J. Hughes, and S. K. Sinha, *Phys. Rev. Lett.* **59**, 2447 (1987).

<sup>9</sup>B. M. Ocko and S. G. J. Mochrie, *Phys. Rev. B* **38**, 7378 (1988).

<sup>10</sup>J. C. Heyraud and J. J. Metois, *Acta Metal* **28**, 1789 (1980).

<sup>11</sup>D. R. Nelson and B. I. Halperin, *Phys. Rev. B* **19**, 2457 (1979).

<sup>12</sup>B. M. Ocko, A. Braslau, P. S. Pershan, J. Als-Nielsen, and M. Deutsch, *Phys. Rev. Lett.* **57**, 94 (1986).

<sup>13</sup>P. S. Pershan, A. Braslau, A. H. Weiss, and J. Als-Nielsen, *Phys. Rev. A* **35**, 4800 (1987).

<sup>14</sup>A. Braslau, P. S. Pershan, G. Swislow, B. M. Ocko, and J. Als-Nielsen, *Phys. Rev. A* **38**, 2457 (1988).

<sup>15</sup>P. W. Palmberg and T. N. Rhodin, *Phys. Rev.* **161**, 586 (1967).

<sup>16</sup>D. M. Zehner, B. R. Appleton, T. S. Noggle, J. W. Miller, J. H. Barret, L. H. Jenkins, and O. E. Schow III, *J. Vac. Sci. Technol.* **12**, 454 (1975).

<sup>17</sup>D. G. Fedak and N. A. Gjostein, *Phys. Rev. Lett.* **16**, 171 (1966).

<sup>18</sup>G. Binnig, H. Rohrer, Ch. Gerber, and E. Stoff, *Surf. Sci.* **144**, 321 (1984).

<sup>19</sup>K. H. Rieder, T. Engel, R. H. Swendsen, and M. Manninen, *Surf. Sci.* **127**, 223 (1983).

<sup>20</sup>F. Ercolessi, E. Tosatti, and M. Parrinello, *Phys. Rev. Lett.* **57**, 719 (1986).

<sup>21</sup>S. R. Andrews and R. A. Cowley, *J. Phys. C* **18**, 6427 (1985).

<sup>22</sup>I. K. Robinson, *Phys. Rev. B* **33**, 3830 (1986).

<sup>23</sup>D. A. Bruce, *J. Phys. Chem. C* **14**, 5195 (1981).

<sup>24</sup>A. M. Afanas'ev, P. A. Aleksandrov, S. S. Fanchenko, V. A. Chaplanov, and S. S. Yakimov, *Acta. Cryst. A* **42**, 116 (1986).

<sup>25</sup>*Tables of Integrals, Series, and Products*, edited by I. S. Gradshteyn and I. M. Ryzhik (Academic, New York, 1965), p. 36. By including an infinitesimal imaginary component to  $Q_z$  this sum can be performed exactly:  $|\sum_{n=0}^{\infty} e^{iQ_z d n}|^2 = |1/\sin(Q_z d/2)|^2$ . Then using Eq. (1.422.3) of this reference, i.e.,  $1/\sin(\pi z) = (1/\pi) \sum_{n=-\infty}^{\infty} (-1)^n/(z-n)$ , we obtain Eq. (3).

<sup>26</sup>For the (001) plane  $\Gamma = a^2/2$ .

<sup>27</sup>I. K. Robinson, W. K. Waskiewicz, R. T. Tung, and J. Bohr, *Phys. Rev. Lett.* **57**, 2714 (1986).

<sup>28</sup>For an unpolarized source and the monochromator  $Q$  vector in the scattering plane,  $P = [1 + \cos^2(2\theta)\cos^2(2\theta_M)]/[1 + \cos^2(2\theta_M)]$  where  $2\theta$  is the scattering angle of the sample and  $2\theta_M$  is the scattering angle of the monochromator.

<sup>29</sup>S. G. J. Mochrie, *J. Appl. Cryst.* **20**, 1 (1988).

<sup>30</sup>Huber Goniometers are manufactured by Huber Diffraktionstechnik G.m.b.H, Rimsting, West Germany.

<sup>31</sup>C. Rottman and M. Wortis, *Phys. Rev. B* **29**, 328 (1984).

<sup>32</sup>J. D. Axe, *Phys. Rev. B* **21**, 4181 (1980).

<sup>33</sup>One obtains a zeroth-order Bessel function if  $Q_x = Q_y = 0$ .

<sup>34</sup>J. R. Smith and A. Banerjee, *Phys. Rev. B* **37**, 10411 (1988).

<sup>35</sup>The value of  $\zeta_1$  obtained from recent nonspecular reflectivity measurements is much smaller.

<sup>36</sup>J. F. Wendelken and D. M. Zehner, *Surf. Sci.* **71**, 178 (1978).

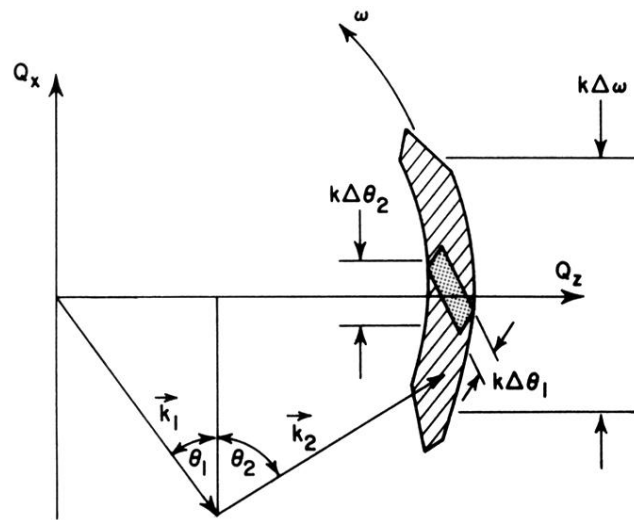


FIG. 1. X-ray resolution volume projected onto the scattering plane. The shaded area is the resolution trapezoid defined by the spread of the incoming beam ( $\Delta\theta_1$ ) and the acceptance of the detector slit ( $\Delta\theta_2$ ). The resolution area swept out by scanning  $\omega$  over a range  $\Delta\omega$  is given by the hatched arc.